A numerical performance assessment of a commercial cardiopulmonary by-pass blood heat exchanger

Filippo Consolo[1*], Gianfranco B. Fiore[1], Alessandra Pelosi[1], Stefano Reggiani[2] and Alberto Redaelli[2]

[1] Dipartimento di Elettronica, Informazione e Bioingegneria, Politecnico di Milano, Piazza Leonardo da Vinci 32, 20133 Milano (MI), Italy; [2]Sorin Group Italia, Via Statale 12 Nord 86, 41037 Mirandola (MO), Italy.

* Corresponding Author:
Filippo Consolo, Ph.D.
Dipatimento di Elettronica, Informazione e Bioingegneria - Politecnico di Milano, Piazza Leonardo da Vinci 32, 20133, Milano (MI) - IT
phone: +39.02.2399.4144
fax: +39.02.2399.3360
email: filippo.consolo@polimi.it

INTRODUCTION

For open-heart surgery that requires cardiopulmonary by-pass (CPB), a blood heat exchanger (BHE) is used to control the patient's blood temperature during the surgery. An integral component of a BHE is a hollow-fiber membrane oxygenator (OXY). In the last few years, the design of cross-flow BHEs based on polymeric hollow-fibers was developed [1]. In those devices, the heating fluid (usually water) is delivered to the inner lumen of the hollow fibers while venous blood is gently channeled through the extracapillary space of the fiber bundle to absorb the necessary heat while passing through the fibers.

Plastic fiber BHEs provide many advantages over the limitations associated with traditional BHEs made with metal (e.g., stainless steel) heating coils [2]. Essentially, the introduction of plastic heating elements dramatically improved the device biocompatibility. In fact, even though they require higher surface contact area to counterbalance the limited heat capacity rate of plastic materials and ensure effective warming of the blood, platelets' contact activation is reduced significantly in plastic fibers. Coating of the fiber surface with proteins/molecules offer enhanced antithrombotic behavior, which is adopted often to further decrease thrombus susceptibility, without compromising the heat exchange efficiency [3]. In addition, in plastic fibers, most of the temperature gradient occurs across the fiber wall thickness rather than at the blood-fiber surface interface, which intrinsically limits the local thermal shock to blood constituents at the fiber wall-adjacent blood layers. Also, plastic hollow-fiber bundles provide a gentle transfer of heat through a stable (as opposed to tortuous, or even turbulent) blood stream, so that, stagnation/recirculation areas eliciting thrombus formation, and high velocity pathways, responsible of non-physiologic shear stress inducing hemolysis and platelet activation, are minimized. Moreover, multiple layers of fibers are packed to form compact size bundles leading to reliable design solutions with reduced priming volumes. Lastly, the use of polymeric fibers results in a faster manufacturing process and comparable manufacturing costs with respect to metal BHE; although metallic heating coils are potentially cheaper than plastic fibers, indeed, the plastic fibers allow assembly of both the OXY

and BHE modules through a one-step manufacturing procedure, namely a single potting of the two fiber bundles.

Nevertheless, the use of plastic fiber bundles introduces the need to preserve a proper spatial arrangement of the fibers to ensure the blood flows uniformly, with minimal resistance/disturbance to flow. Indeed, flow shunting can result from preferential pathways for blood flow caused by inadequate fit of the fiber bundle to the supporting case or from regions of non-uniform fiber packing within the bundle [4]. In those situations, the blood could partially (or entirely) bypass the fiber mat without being adequately heated before re-infusion into the patient, eventually degrading or totally compromising the device efficacy. To prevent the onset of such undesired conditions, convenient geometrical design solutions must be considered.

The present work is a performance assessment study aimed at identifying a convenient design solution of a new commercial plastic fiber BHE integrated into a hollow-fiber OXY, called INSPIRE^{TM}, recently released by Sorin Group Italia (SGI) and intended for use in adult patients during open-heart surgery. Within the device, transverse blood flow was established, enabling multiple passages of the blood through the fibers to enhance heat exchange efficiency, without any relevant increase in device priming volume or in blood-surface contact area with respect to currently available BHEs. In a comparative analysis, the hemo- and thermo-dynamics performance of five different prototypical BHE geometries were evaluated. The five different configurations were conceived by SGI as possible design solutions addressing the multiple technical requirements of BHEs, and, in particular, in order to effectively support the polymeric fiber bundle. Through a numerical approach based on multi-physics computational fluid dynamics (CFD) simulations, we identified the design solution complying with the most convenient trade-off in terms of i) uniformity of blood flow patterns within the fiber bundle to prevent blood flow shunting and the formation of stagnation/recirculation areas and/or turbulent blood flow; ii) enhancement of heat transfer efficiency; iii) minimization of pressure drops and vi) minimization of priming volume, as

general design requirements for any CPB device. The selected design was then prototyped and tested and *in vitro* data were compared with respect to CFD predictions.

MATERIALS AND METHODS

1. Device description

The device (Fig. 1A-C) consists of two pseudo-cylindrical polymeric hollow-fiber bundles (OXY: polypropylene, BHE: polyurethane fibers) coaxially arranged within the external housing where the blood inlet and outlet ports are located. In particular, the bundle of the BHE unit is housed within a cylindrical external shell and an inner core connected to the inlet port facilitating the blood to be pre-heated in the BHE fiber bundle. The inner and outer surfaces of the BHE are provided with six longitudinal ribs each, which provide vanes between the hollow fiber bundle and the inner cylindrical core and the outer shell, respectively. Such vanes are spatially arranged to impart a radial component to the blood flow, a characteristic design solution that allowed establishing transversal blood flow with multiple passages of the blood across the fibers. The inner ribs also work as a support structure for the fiber bundle, preventing the protrusion of the fibers within the vanes, thus avoiding any obstruction to blood flow. The bundle of the BHE module is then interfaced with the OXY bundle through eight equally spaced rectangular windows allowing the blood to flow around and across the fibers. A comprehensive description of the device, including characteristics of the fibers of the OXY and BHE modules, can be found in [5].

Five different geometries of the BHE module (Fig. 1D) were conceived during the design stage. Starting from a baseline module (M1), used as a comparison, four design alternatives were evaluated as subsequent modifications of the BHE inner core. The progressive enlargement of the internal ribs (M2), the tightening of the vanes (M3), the introduction of central supports within the vanes (M4), and the use of a frame overlapped to the ribs (M5) were all designs dictated by the need to have an effective support preventing fiber bundle protrusion and blood flow shunting.

2. CFD analysis

In this section the main steps of the multi-physics CFD analysis performed on the five BHE prototypes will be described. While fluid- and thermo-dynamic analyses were conducted, it should be noted that the two analyses were performed simultaneously, using the commercial software ANSYS FLUENT v13.0 (ANSYS Inc., Canonsburg, USA).

2.1. 3D fluid modeling

The 3D fluid volumes within the five BHE prototypes (Fig. 2, M1-M5) were reconstructed and discretized (see Supplementary Material, section 1. Fluid-dynamic analysis) using ANSYS Design Modeler and the Meshing module of ANSYS Workbench v.13.0 (ANSYS Inc., Canonsburg, USA). Since no design modifications were applied to the OXY module, only the inlet portion of the OXY fiber bundle (about one tenth of the total bundle length) was modeled to ensure the correct boundary conditions at the BHE outlet. Physical dimensions of the fluid volumes are reported in Table 1.

2.2. Fluid-dynamic analysis

The fluid-dynamic analysis was aimed at evaluating blood pressure drops across the BHE and to gain insight into the blood flow pattern in each of the prototypical geometries. For all the CFD simulations, a blood flow rate (Q_b) equal to 5 L/min was assumed, corresponding to a velocity equal to 1.25 m/s applied at the inlet section (Fig. 3A), while zero pressure outlet and no-slip conditions were set at the walls. Blood was modeled as an incompressible Newtonian fluid, with a 1052 kg/m^3 density value; a user-defined function (UDF) was written to implement the temperature-dependent behavior of the blood viscosity (μ_b), according to Einstein's equation [5], assuming that particles did not interact with each other (eq. 1):

$$\mu_b = (1 + 2.5\mathrm{Ht}) \cdot 1.8 \frac{\mu_0}{(1 + 0.0337 \cdot \mathrm{T} + 0.00022 \cdot \mathrm{T}^2)} \qquad (1)$$

where Ht is the hematocrit, equal to 34%, a typical condition for diluted blood during CPB and μ_0 is the viscosity of water at the reference temperature (T) of 0°C.

To avoid the computational cost required to model every single fiber in the devices [7,8], a porous media model was adopted to simulate the OXY and BHE fiber bundles, adding a momentum sink term (S) to the standard fluid flow equation (eq. 2, 3):

$$\rho\frac{\partial V}{\partial t}+\rho V\cdot \mathrm{grad}(V)=-\mathrm{grad}(P)+\eta\nabla^2 V+\rho g+S \qquad (2)$$

where:

$$S_i=-\left(\frac{\eta}{\alpha}v_i+\frac{1}{2}C_2\rho|v_i|v_i\right) \qquad (3)$$

At low flow rates (Q<6 L/min), the second term in eq. 2, accounting for inertial effects, can be neglected [8]. Thus, the characteristics of the porous model depend only on its viscous resistance $1/\alpha$, according to Darcy's Law. To determine $1/\alpha$, experimental tests were performed at the SGI laboratories [8]. Briefly, the devices were perfused with bovine blood at 34% hematocrit and 37 °C, with Q_b ranging from 2 to 6 L/min, and $1/\alpha$ was calculated as (eq. 4):

$$\frac{1}{\alpha}=\frac{A\cdot\Delta P}{\eta\cdot Q\cdot L} \qquad (4)$$

where A and L are the transversal cross section and the length of the fiber bundle, respectively, and ΔP is the pressure drop across the fiber bundle.

2.3. Thermo-dynamic analysis

The aim of the thermo-dynamic analysis was to evaluate the heat exchange efficiency (ε) of each BHE prototype. The Dual Cell computational scheme, based on the ε-NTU method was adopted to compute the total heat transfer (see Supplementary Material, section 2. Thermo-dynamic analysis) [9]. Accordingly, the thermal domain was modeled by two overlapping volumes, having distinct but exactly superimposed meshes: one for the primary fluid zone (blood) and one for the auxiliary fluid zone (water). The auxiliary fluid zone was split longitudinally into two halves in order to mimic the double passage of the water flowing within the BHE bundle (Fig. 3B). The blood (T_{b_in}) and water (T_{w_in}) inlet temperatures were set to 30°C and 40°C, respectively; the water flow rate was equal to 10 L/min for each simulation. To ensure the physical coherence of the results, ε was computed (eq.

5) on the outlet surface of the device using the outlet blood temperature weighted-averaged with respect to the blood outlet velocity ($\overline{T}_{b\_out}$):

$$\varepsilon = \frac{\overline{T}_{b\_out} - T_{b\_in}}{T_{w\_in} - T_{b\_in}} \quad (5)$$

3. Prototyping and experimental characterization

The best-performing BHE design solution, identified according to CFD predictions, was prototyped and an experimental campaign was carried out at SGI laboratories, according to ISO 7199:2009 standard [10] and FDA 510(K) guidance [11], aimed at characterizing the device performances *in vitro*. Five different prototypes were individually tested. The devices were perfused with bovine blood (34% hematocrit) at 5 L/min flow rate, with a 10-L/min heating water flow rate. Blood and water temperature at the inlet and outlet ports of the BHE were monitored to calculate ε (see Supplementary Material, section 3. The experimental layout for BHE characterization).

RESULTS

Computational results were post-processed to extract spatial dependent quantities, such as blood velocity, pressure drop and temperature maps, in order to identify the BHE core design solution that better accommodated the trade-off between hemo- and thermo-dynamic performances.

The contour maps of the velocity magnitude and temperature distribution within the five investigated designs are displayed in Figure 4. In Table 2, the values of the maximum blood temperature (T_{b_max}), the outlet blood temperature ($\overline{T}_{b\_out}$), the overall heat exchange efficiency (ε) and pressure drop in the BHE bundle (ΔP, calculated as the difference between the pressure at the entrance of the BHE bundle, i.e. at the interface between the BHE bundle and the flow distributor, and the exit section of the BHE bundle, i.e. at the interface between the BHE and the OXY volumes, Fig. 2B) are reported.

According to our results, the blood velocity pattern is characterized by i) low velocity areas mostly located in the bundle central region, where the residence (and therefore the heating) time of the blood threads that cross the fibers increases, and ii) a preferential high-velocity path on the distal external side of the bundle (zoomed-in areas, Fig. 4), causing the high velocity blood threads to absorb less heat before reaching the outlet of the BHE bundle. Coherently, the analysis of the temperature maps (Table 2) highlighted that the temperature computed at the outlet section of the BHE bundle ($\overline{T}_{b\_out}$), being the result of different blood threads mixing, was slightly lower than the maximum temperature (T_{b_max}) within the BHE bundle, located at an internal section in the central distal part of the BHE fibers bundle. Although this pattern was observed for all of the investigated prototypes, the different geometrical configurations characterizing the five prototypes of the BHE internal core significantly influence the device performance, resulting in different values of $\overline{T}_{b\_out}$ and ε (Table 2). In particular, the M4 and M5 prototypes exhibited the highest values of $\overline{T}_{b\_out}$ (36.54 °C and 36.56 °C, respectively) and ε (65.40% and 65.60%, respectively) with respect to the alternative configurations.

M4 and M5 were characterized by comparable heat exchange performances; however, significant differences were observed in their blood flow pathway. In detail, an altered and heterogeneous distribution of the blood velocity pattern was observed in M4: due to the complex fish-bone-shaped supports within the vanes, leaning against the fiber bundle, high blood velocity peaks (maximum velocity = 1.30 m/s) are generated within the fiber bundle at the level of the vanes (Fig. 5A). Furthermore, such a heterogeneous fluid-dynamic condition is responsible for elevated ΔP values computed for M4 (45.3 mmHg). On the contrary, in M5 (Fig. 5B), the overlapped external frame characterized by rounded holes do not alter the fluid-dynamics within the vanes and only slightly affect the entrance of the blood in the bundle, which uniformly flows across the fibers: in fact, no high velocity blood threads were detected (maximum velocity = 0.43 m/s); consequently, M5 is characterized by lower ΔP values with respect to the alternative models (Table 2). Concerning ΔP,

it is worth noting that the pressure distribution in the bundle depends only on the fluid pattern generated in each specific design geometry, since the permeability coefficient of the fiber bundle, according to the porous media assumption (eq. 3), was the same throughout the study. The comparison of ΔP revealed that M5 had the lowest value (37.5 mmHg), with the exception of M1 only (34.4 mmHg). Nevertheless, the external solid frame overlapped the BHE core of M5 guaranteeing a better support for the fibers with respect to M1, thus limiting the risk of bundle protrusion and blood flow shunting.

All together, our results indicate M5 as the best performing BHE configuration, which was prototyped and tested. Experimental data (see Supplementary Material, section 3. The experimental layout for BHE characterization) confirmed the results of the numerical analysis, which accurately estimated the thermo-dynamic BHE performances, revealing minimal differences between the measured and the computed ε values ($\varepsilon_{\_EXP}$ = 65.25%±0.64% *vs* $\varepsilon_{\square CFD}$ = 65.60%).

DISCUSSION

Recently introduced polymeric BHEs offer new design perspectives with respect to metal coil-based BHEs. Indeed, even with heat transfer coefficients as low as those typical of polymers (stainless-steel thermal conductivity = 22 $W\,m^{-1}\,k^{-1}$, whereas polymers range two orders of magnitude lower, e.g., 0.23 $W\,m^{-1}\,k^{-1}$ for polyurethane), appropriate heat transfer may still be obtained if one properly dimensions the fiber wall thickness and the exchange surface area. In addition, compact-size bundles can be realized through modern manufacturing techniques avoiding any dramatic increase of the device volume. Those considerations are summarized in Table 3, comparing the specifications and performance data of some representative metallic and polymeric BHE modules currently on the market for CPB application, including the M5 BHE model conceived in this study. In addition, with specific reference to the continuous enhancement of device safety, plastic BHEs are intrinsically safer, improving the patients' outcome following CPB [12].

With this novel approach, evidently finding an optimal trade-off between different design needs has become a more refined challenge that benefits from the use of advanced numerical modeling, rather than time-consuming and costly procedures based on the subsequent manufacturing of multiple physical prototypes and testing. CFD-based design optimization was demonstrated to be a valuable and an effective tool to support the performance analysis and optimization of blood handling medical devices. It is, to date, widely used in industrial design processes [8,12-24], and its significance was recently recognized by the FDA [25, 26]. The advantages of CFD-based virtual design and prototyping all turn into more successful performances [27]. In fact, CFD allows to quantitatively estimate parameters of interest which are difficult to evaluate or immeasurable by experimentation, providing an ideal but accurate performance measurement system not otherwise attainable and it is believed that "through standardized computational modeling techniques, the design, testing, and regulatory review of medical devices or components will lead to improvements in efficacy and cost throughout the pre-market and post-market stages of the product's life cycle" [27].

According to those considerations, in this study the development of a multi-physics CFD-based numerical model demonstrated to be particularly valuable to compare the hemo- and thermo-dynamics performance of the specific BHE model we analyzed. Typical industrial empirical design methodologies, indeed, allow for a mere qualitative evaluation of the flow field within the fibers, mainly due to the structure and opacity of the fibers themselves [21]. Conversely, CFD simulations allow an insightful visualization of the blood flow within the bundle and this allows the identification and the ability to uncover different critical aspects related to the device geometry to be improved in the manufacturing phase. CFD simulations permit the extraction of geometrical-dependent quantitative parameters to be used in the comparative analysis of the five candidate designs, dramatically increasing awareness during the BHE design optimization stage. Furthermore, the multi-physics numerical analysis allowed us to perform a comprehensive evaluation of the major design criteria affecting the device performance, taking into account both the hemo- and

thermo-dynamic performance. Indeed, our results concerning heat transfer *per se* give some interesting view of how our five candidate configurations perform as a whole. With a combined hemo- and thermo-dynamic performance evaluation of each candidate model, it was possible to critically compare those design solutions that seemingly appeared equivalent. For instance, the design modifications of the ribs/vanes profile provided in the M2 and M3 models, although resulting in comparable values of ε with respect to M1 (small percent differences were detected), were responsible for significantly higher ΔP across the bundle. This definitely suggested that the M2 and M3 configurations were far from addressing the multiple technical requirements we defined for the BHE performance optimization. Similarly, when comparing M4 and M5 models, we were able to make a definite choice based on their inner flow patterns, although they had equivalent heat exchange performances.

The selected BHE model (M5) ameliorated efficacy and reliability with respect to alternative polymeric BHE models currently available on the market; in particular, thanks to its characteristic design geometry, comparable heat exchange efficacy was achieved with reduced heat exchanger surface area and device priming volume (Table 3).

The M5 was prototyped to experimentally characterize the device performance and a good agreement was found between the results obtained from computational and experimental evaluation, proving that the techniques employed in this work are appropriate, and the effectiveness of the numeric tool we developed to assist the design and manufacturing phase of blood handling medical devices was adequate. In addition, the proposed approach could be extended to similar applications in which the determination of the design requirements is strongly based on fluid-dynamic patterns.

In conclusion, multiphysics CFD-based simulations accurately predicted both the hemo- and thermo-dynamic performance of the BHE we analyzed, allowing us to identify the best performing solution among five different investigated prototypes on the basis of quantitative geometrical-dependent parameters not derivable from empirical methods. Remarkably, the computer-aided

design strategy limited the need of iterative prototyping, with a beneficial effect upon the overall design process and time-to-market. However, the presented numerical tool suffers from some limitations, such as the lack of quantitative evaluation of the thrombogenic potential associated with the blood flow path within the device. Further studies are therefore required that aim at enhancing the device biocompatibility in terms of minimization of the patients' side effect during CPB.

ACKNOWLEDGEMENTS: The authors would like to thank Claudio Silvestri and Antonia Saraceno of Sorin Group Italia for providing the experimental data.

Competing Interests

Stefano Reggiani is employee of Sorin Group Italia. For the remaining authors none were declared.

Please state any sources of funding for your research

Sorin Group Italia provided fees for computer simulation to Filippo Consolo, Gianfranco B Fiore, Alessandra Pelosi and Alberto Redaelli.

If your study involves human subjects you MUST have obtained ethical approval. Please state whether Ethical Approval was given, by whom and the relevant Judgement's reference number

The study does not involve human subjects. No Ethical Approval was thus required.

REFERENCES

[1] Segers PA, Heida JF, de Vries I, Maas C, Boogaart AJ and Eilander S: Clinical evaluation of nine hollow-fibre membrane oxygenators. Perfusion 2001; 16:95-106.

[2] Elgas RJ: Investigation of the phenomenon of electrostatic compromise of a plastic fiber heat exchanger. Perfusion 1999; 14:133-140.

[3] Belway D, Rubens FD: Currently available biomaterials for use in cardiopulmonary bypass. Expert Rev Med Devices 2006; 3:345-55.

[4] Haworth WS: The development of the modern oxygenator. Ann Thorac Surg 2003; 76:2216-2219.

[5] http://www.sorin.com/sites/default/files/product/files/2014/03/12/inspire_6_brochure_en.pdf

[6] Mueller S, Llewellin EW, Mader HM: The rheology of suspensions of solid particles. Proceedings of the Royal Society A: Mathematical, Physical and Engineering Sciences 2010; 466:1201-1228.

[7] Gage KL, Gartner MJ, Burgreen GW, Wagner WR: Predicting membrane oxygenator pressure drop using computational fluid dynamics. Artif Organs 2002; 26:600-607.

[8] Pelosi A, Sheriff J, Stevanella M, Fiore GB, Bluestein D, Redaelli A: Computational evaluation of the thrombogenic potential of a hollow-fiber oxygenator with integrated heat exchanger during extracorporeal circulation. Biomech Model Mechanobiol 2013; 13:349-361.

[9] Incropera FP, DeWitt DP, Bergman TL, Lavine AS: Fundamentals of Heat and Mass Transfer, 6th edition. John Wiley & Sons, NJ, 2006.

[10] http://www.iso.org/iso/catalogue_detail.htm?csnumber=51030.

[11]http://www.fda.gov/MedicalDevices/DeviceRegulationandGuidance/GuidanceDocuments/ucm0736.

[12] Asakawa Y, Funakubo A, Fukunaga K, Taga I, Higami T, Kawamura T, Fukui Y: Development of an implantable oxygenator with cross-flow pump. ASAIO J 2006; 52:291-295.

[13] Fill B, Gartner M, Johnson G, Horner M, Ma J: Computational fluid flow and mass transfer of a functionally integrated pediatric pump-oxygenator configuration. ASAIO J 2008; 54:214-219.

[14] Graefe R, Borchardt R, Arens J, Schlanstein P, Schmitz-Rode T, Steinseifer U: Improving oxygenator performance using computational simulation and flow field-based parameters. Artif Organs 2010; 34:930-936.

[15] Fraser KH, Zhang T, Taskin ME, Griffith BP, Wu ZJ: Computational fluid dynamics analysis of thrombosis potential in left ventricular assist device drainage cannulae. ASAIO J 2010; 56:157-163.

[16] Hormes M, Borchardt R, Mager I, Schmitz-Rode T, Behr M, Steinseifer U: A validated CFD model to predict O_2 and CO_2 transfer within hollow fiber membrane oxygenators. Int J Artif Organs 2011; 34:317-325.

[17] Gage KL, Gartner MJ, Burgreen GW, Wagner WR: Predicting membrane oxygenator pressure drop using computational fluid dynamics. Artif Organs 2007; 26:600-607.

[18] Fiore GB, Redaelli A, Guadagni G, Inzoli F, Fumero R: Development of a new disposable pulsatile pump for cardiopulmonary bypass: computational fluid-dynamics design and in vitro tests. ASAIO J 2002; 48:260-267.

[19] Fill B, Gartner M, Johnson G, Horner M, Ma J: Computational fluid flow and mass transfer of a functionally integrated pediatric pump-oxygenator configuration. ASAIO J 2008; 54:214-219.

[20] Fiore GB, Morbiducci U, Ponzini R, Redaelli A. Bubble tracking through computational fluid dynamics in arterial line filters for cardiopulmonary bypass. ASAIO J 2009; 55:438-444.

[21] Bhavsar SS, Schmits-Rode T, Steinsfeier U: Numerical modeling of anisotropic fiber bundle behavior in oxygenators. Artif Organs 2011; 35:1095-1102.

[22] Fraser KH1, Taskin ME, Griffith BP, Wu ZJ. The use of computational fluid dynamics in the development of ventricular assist devices. Med Eng Phys. 2011; 33(3):263-80.

[23] Carswell D1, Hilton A, Chan C, McBride D, Croft N, Slone A, Cross M, Foster G. Development of a radial ventricular assist device using numerical predictions and experimental haemolysis. Med Eng Phys. 2013; 35(8):1197-203.

[24] Zhang J, Zhang P, Fraser KH, Griffith BP, Wu ZJ: Comparison of fluid dynamic numerical models for a clinical ventricular assist device and experimental validation. Artif Organs 2013; 37: 380-389.

[25]http://www.fda.gov/MedicalDevices/DeviceRegulationandGuidance/GuidanceDocuments/ucm371016.htm.

[26]http://www.fda.gov/scienceresearch/specialtopics/criticalpathinitiative/spotlightoncpiprojects/ucm149414.htm.

[27] https://www.asme.org/engineering-topics/articles/performance-test-codes/improving-medical-devices-using-computational-mode.

FIGURE CAPTIONS

Figure 1: Internal view CAD 3D drawings of the INSPIRE^{TM} blood OXY-HE module showing **(A)** the OXY fiber bundle, **(B)** the OXY internal core and the outer and inner solid cores surrounding the BHE fiber bundle; **(C)** cross-sectional view showing a cut-away portion of the device in the longitudinal plane; **(D)** CAD 3D drawings of the five different prototypes of the BHE internal core.

Figure 2: The 3D fluid domain of the OXY and BHE baseline (M1) module **(A)**; in **(B)** the sole BHE fluid domain is depicted to allow visualization of the BHE-OXY interface geometry; **(C)** internal cross-sectional view (z-x plane) showing the BHE internal vanes (M1); **(D)** blood pathlines are depicted on an internal cross-sectional view (z-x plane) of the M1 model, sketching schematically the flow pattern imparted to the fluid within the device: pathlines highlight the transversal blood flow path within the fiber bundle, enabling multiple passages of the blood through the fibers; **(E)** internal cross-sectional view (z-x plane) of the fluid domain of the five BHE prototypes, labeled with respective model ID. In Fig. 2C and 2E the fiber bundle of the OXY and BHE modules is light-red colored.

Figure 3: Boundary flow conditions are shown for blood **(A)** and water **(B)** with velocity inlet, pressure outlet, wall surfaces and the porous zone colored in blue, red, dark grey, and light grey respectively.

Figure 4: Contour maps of velocity magnitude **(top)** and temperature distribution **(bottom)** plotted in a representative longitudinal internal plane (z-x plane) of the five BHE models (M1-M5).

Figure 5: Contour maps of velocity magnitude **(left**, color scales are set at the maximum velocity value computed for the M4 model**)** and temperature distribution **(right)** plotted on the external surface of three different volume zones of M4 **(A)** and M5 **(B)** configurations. The red rectangle in **(A)** highlights the areas of M4 where high-velocity blood threads were detected.

LIST OF TABLES

Dimension	Value [mm]
Height (BHE + inlet conduit)	171.5
BHE core height	137
BHE core diameter	26.8
BHE fiber bundle height	137
BHE fiber bundle thickness	7.7
OXY fiber bundle height	13.7
OXY fiber bundle thickness	10.5
Inlet diameter	9.23

Table 1: Physical dimensions of the fluid volumes of the M1-M5 prototypes.

Model ID	T_{b_max} [°C]	$\overline{T}_{b\_out}$ [°C]	ε [%]	ΔP [mmHg]
M1	37.34	36.36	63.60	34.40
M2	37.37	36.32	63.20	42.30
M3	37.77	36.16	61.60	68.00
M4	37.47	36.54	65.40	45.30
M5	37.37	36.56	65.60	37.50

Table 2: Maximum blood temperature detected in correspondence with an internal section of the BHE bundle (T_{b_max}), blood temperature at the outlet section of the BHE bundle ($\overline{T}_{b\_out}$), overall thermal exchange efficiency (ε) and pressure drops (ΔP) are reported for each model.

	Type of heat exchanger	Heat exchanger Surface Area [m^2]	ε [%]	Priming Volume [ml]
Dideco D903 Avant	Stainless steel	0.17	55 (Q_b = 6 L/min) (Q_w = 10 L/min)	270
Dideco Compactflo EVO	Stainless steel	0.14	55 (Q_b = 6 L/min) (Q_w = 10 L/min)	250
Sorin Group Primox	Stainless steel	0.14	50 (Q_b = 6 L/min) (Q_w = 10 L/min)	250
Sorin Synthesis	Stainless steel	0.14	49 (Q_b = 6 L/min) (Q_w = 10 L/min)	430 (with arterial filter)
Sorin APEX HP	Stainless steel	0.17	54 (Q_b = 6 L/min) (Q_w = 10 L/min)	250
Terumo Capiox RX25	Stainless steel	0.2	55 (Q_b = 6 L/min) (Q_w = 15 L/min)	250

Terumo Capiox FX25	Stainless Steel	0.2	55 (Q_b = 6 L/min) (Q_w = 15 L/min)	260
Medtronic Affinity NT	Stainless Steel	0.168(*)	45 (Q_b = 6 L/min) (Q_w = 10 L/min)	270
Eurosets Admiral	Stainless Steel	0.08	64 (Q_b = 4 L/min) (Q_w = 10 L/min)	190
Eurosets AMG	Stainless Steel	0.08	64 (Q_b = 4 L/min) (Q_w = 10 L/min)	220
Maquet Jostra Quadrox	Polyurethane	0.60	69 (Q_b = 6 L/min) (Q_w = 10 L/min)	250
Maquet Jostra Quadrox - D	Polyurethane	0.60	69 (Q_b = 6 L/min) (Q_w = 10 L/min)	250
Maquet Jostra Quadrox-i adult	Polyurethane	0.40	67 (Q_b = 6 L/min) (Q_w = 10 L/min)	215

Medos Hilite 7000	Polyester	0.45	60 (Q_b = 6 L/min) (Q_w = 10 L/min)	275
Medtronic Affinity Fusion	Polyethylene terephthalate	0.40	65 (Q_b = 6 L/min) (Q_w = 10 L/min)	260
Sorin Group INSPIRE (M5 model)	Polyurethane	0.34	65.6 (Q_b = 5 L/min) (Q_w = 10 L/min)	178

Table 3: Specifications data of different metallic and polymeric BHEs currently on the market and of the five polymeric BHE prototypes (M1-M5) analyzed in this study. Priming volume values refer to the integrated OXY+BHE modules. Data for commercial devices were estimated from the product brochures, except (*): from.[1] Q_b and Q_w are the blood and water flow rates, respectively.

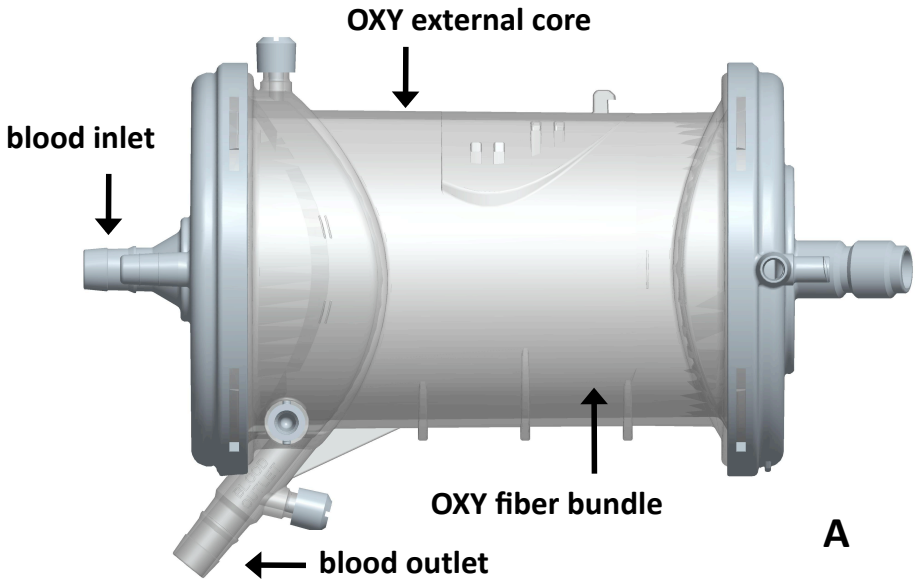
OXY external core
blood inlet
OXY fiber bundle
blood outlet
A

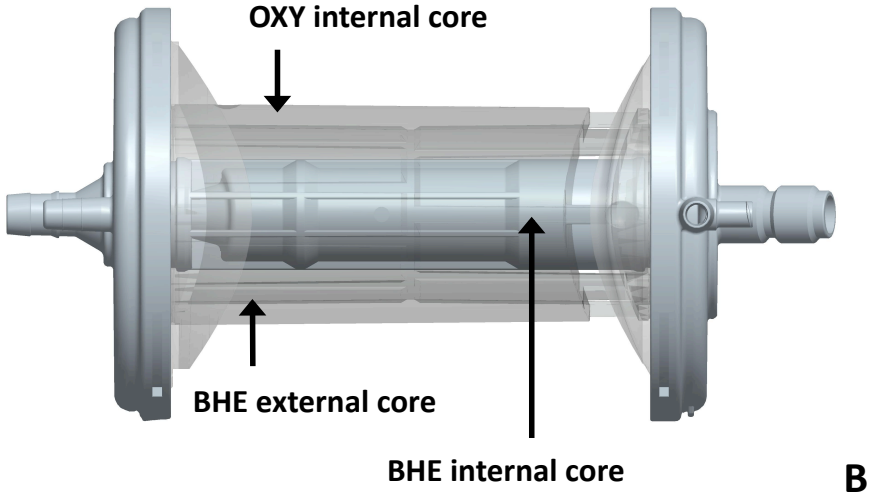
OXY internal core
BHE external core
BHE internal core
B

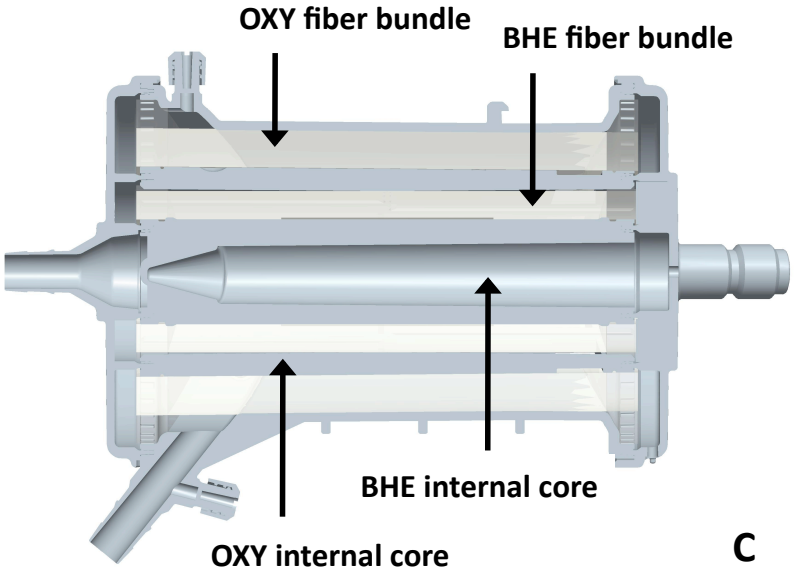
OXY fiber bundle
BHE fiber bundle
BHE internal core
OXY internal core
C

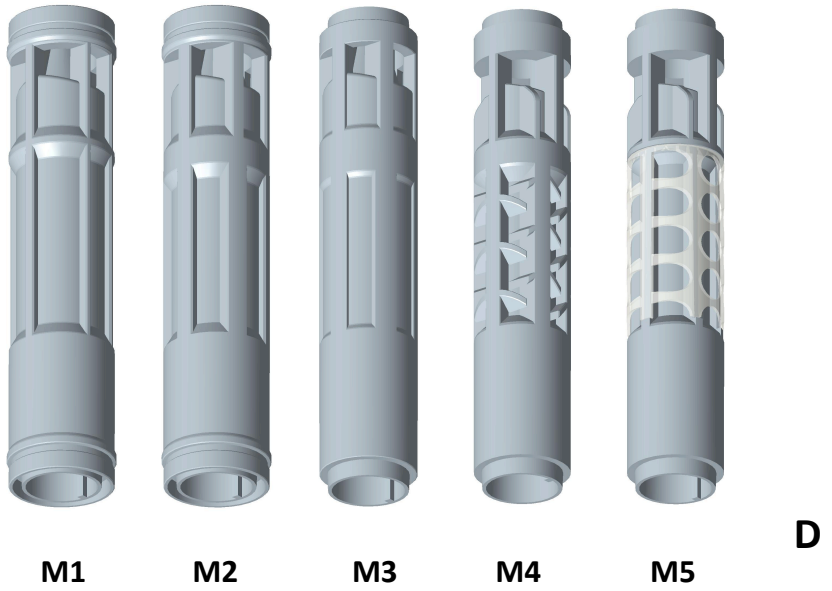
M1
M2
M3
M4
M5
D

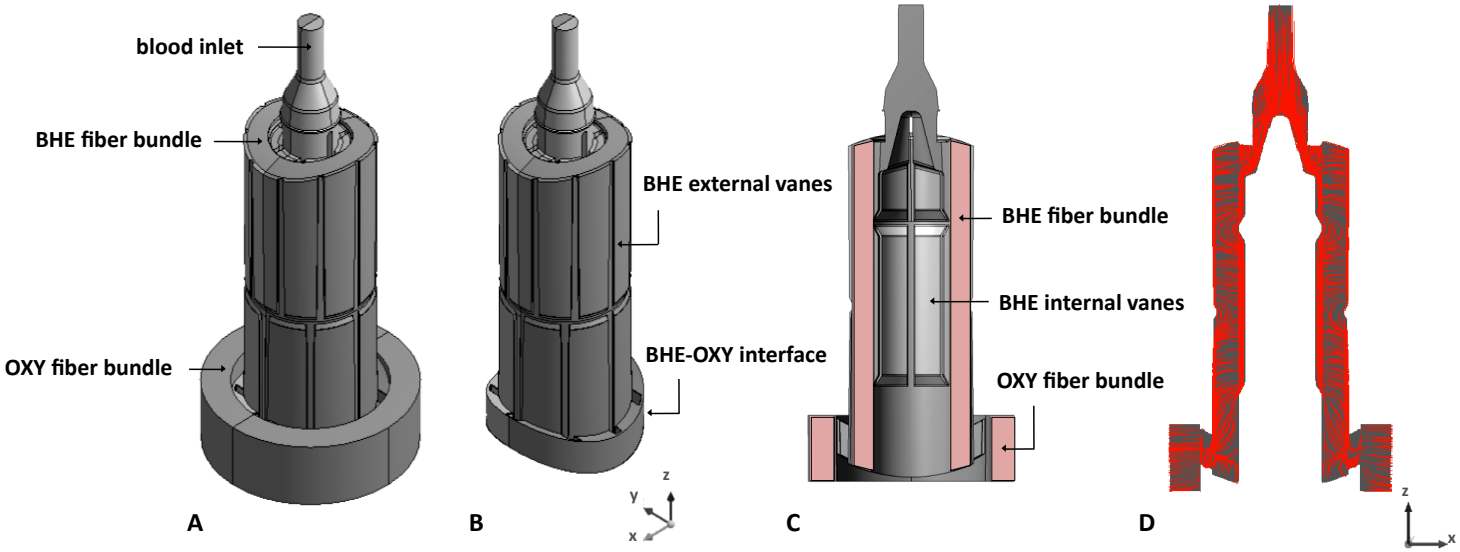
blood inlet
BHE fiber bundle
OXY fiber bundle
A
BHE external vanes
BHE-OXY interface
B
BHE fiber bundle
BHE internal vanes
OXY fiber bundle
C
D

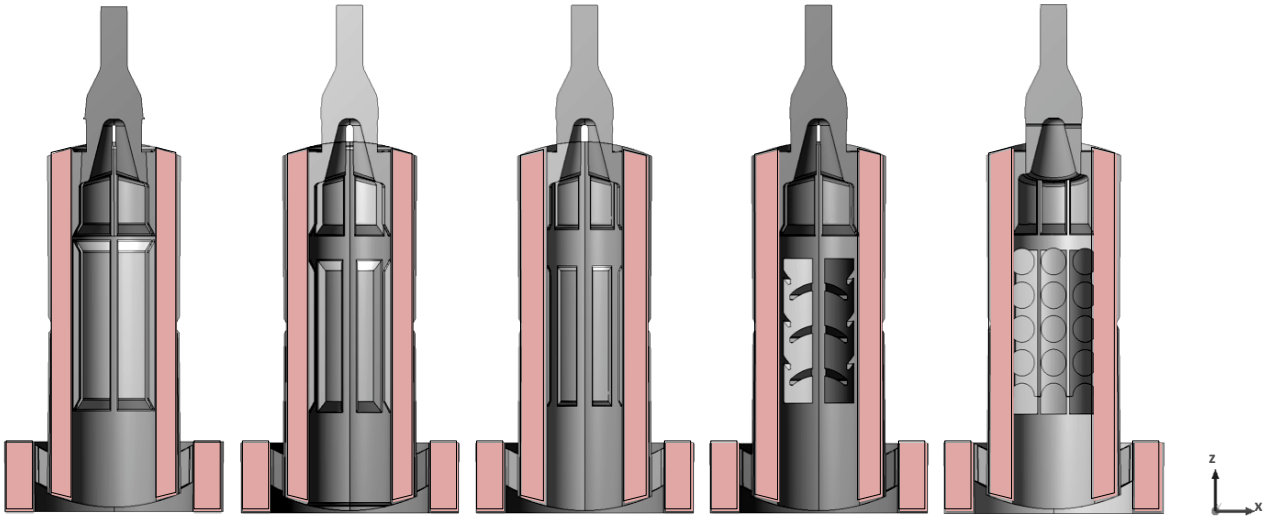
M1
M2
M3
M4
M5
E

Figure_3

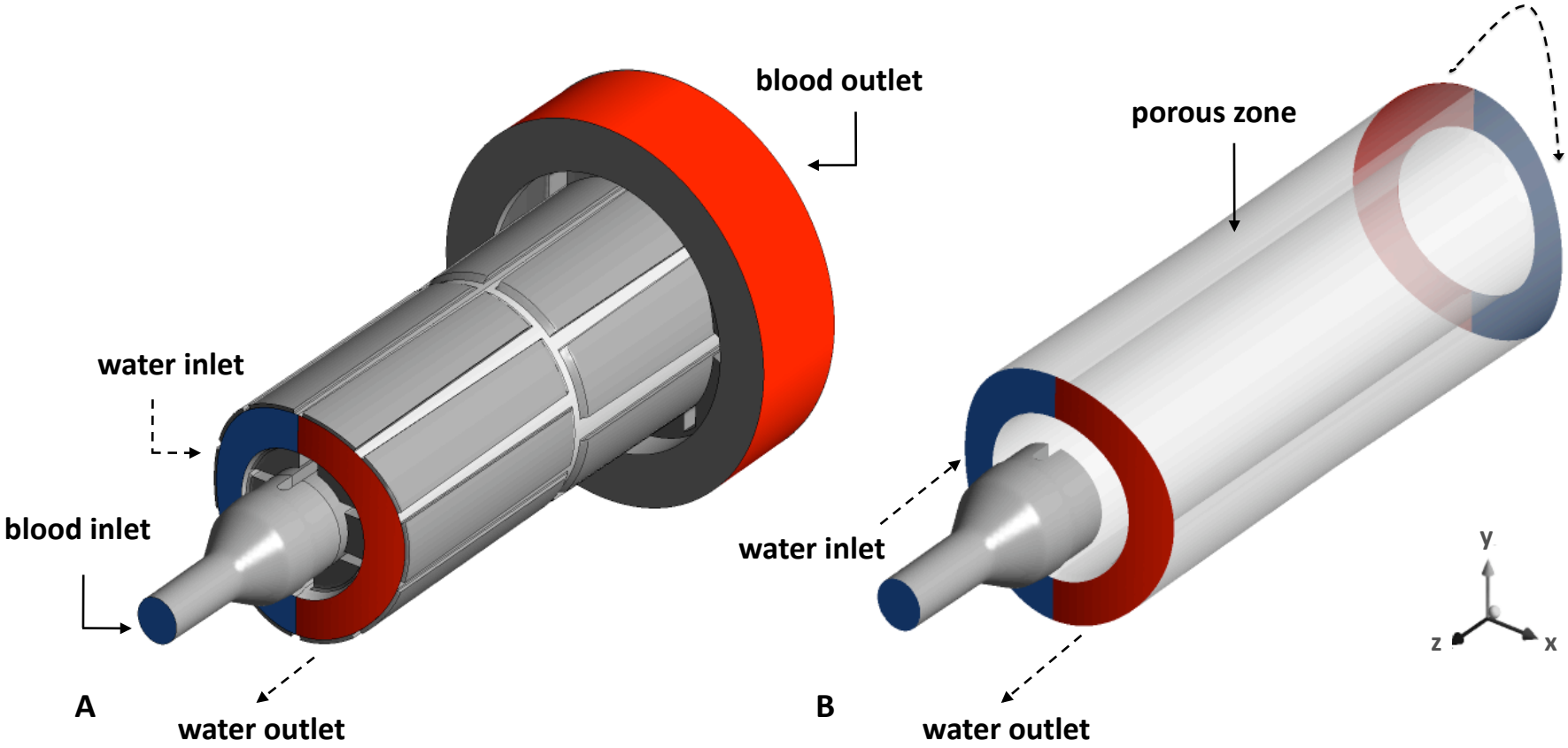
blood outlet
water inlet
blood inlet
A
water outlet
porous zone
water inlet
B
water outlet
y
z
x

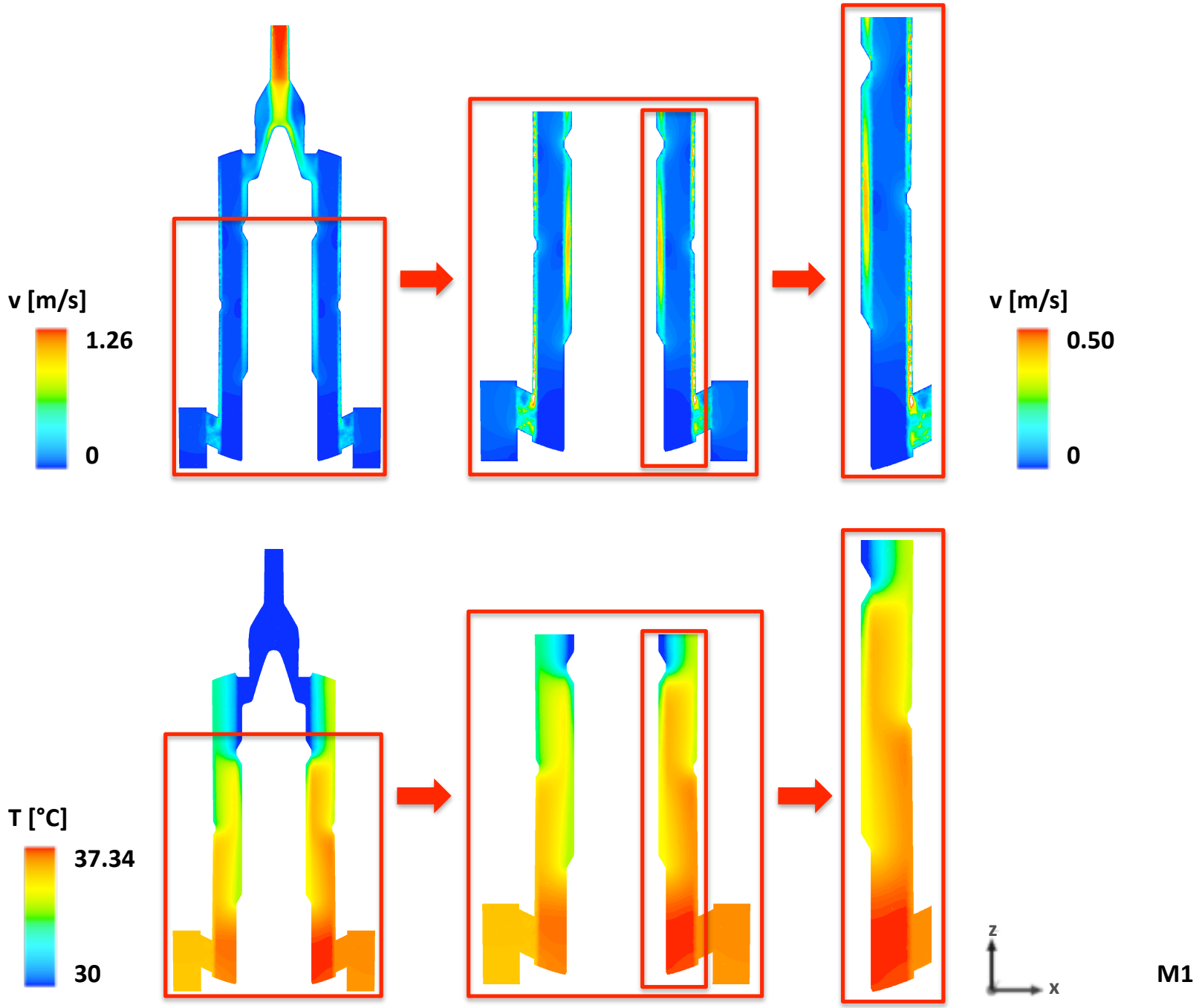
v [m/s]
1.26
0
v [m/s]
0.50
0
T [°C]
37.34
30
z
x
M1

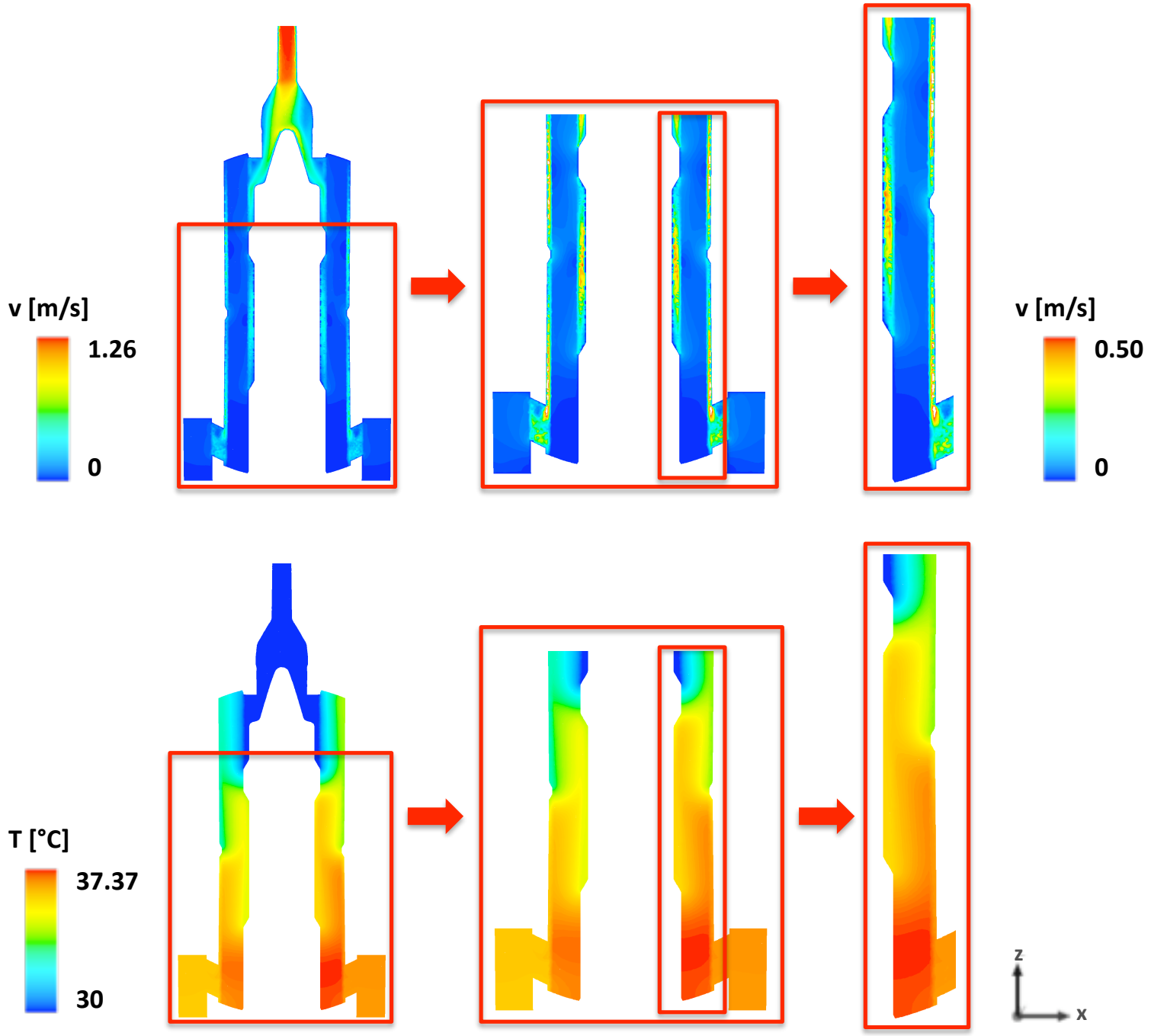
v [m/s]
1.26
0
v [m/s]
0.50
0
T [°C]
37.37
30
z
x
M2

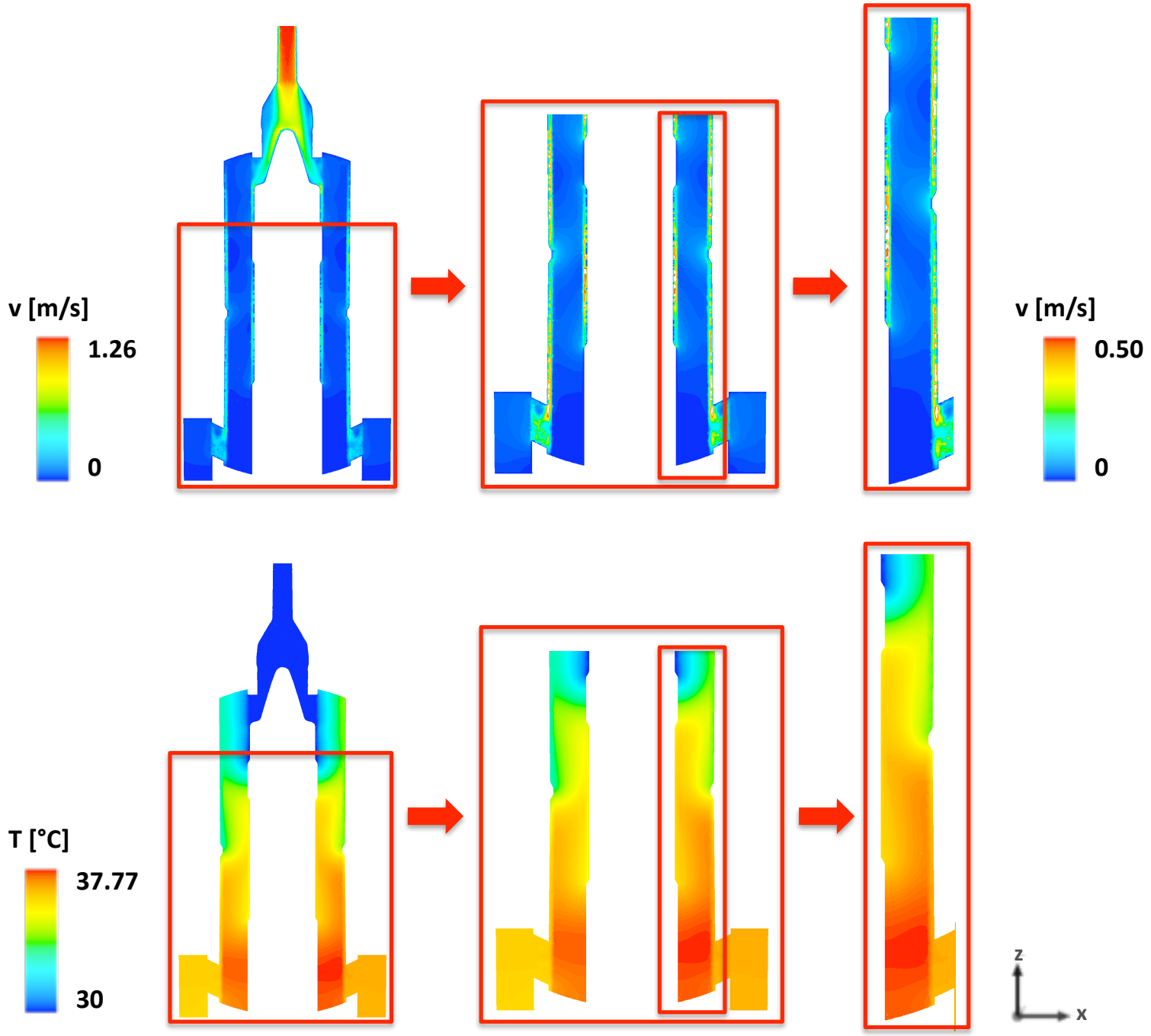
v [m/s]
1.26
0
v [m/s]
0.50
0
T [°C]
37.77
30
z
x
M3

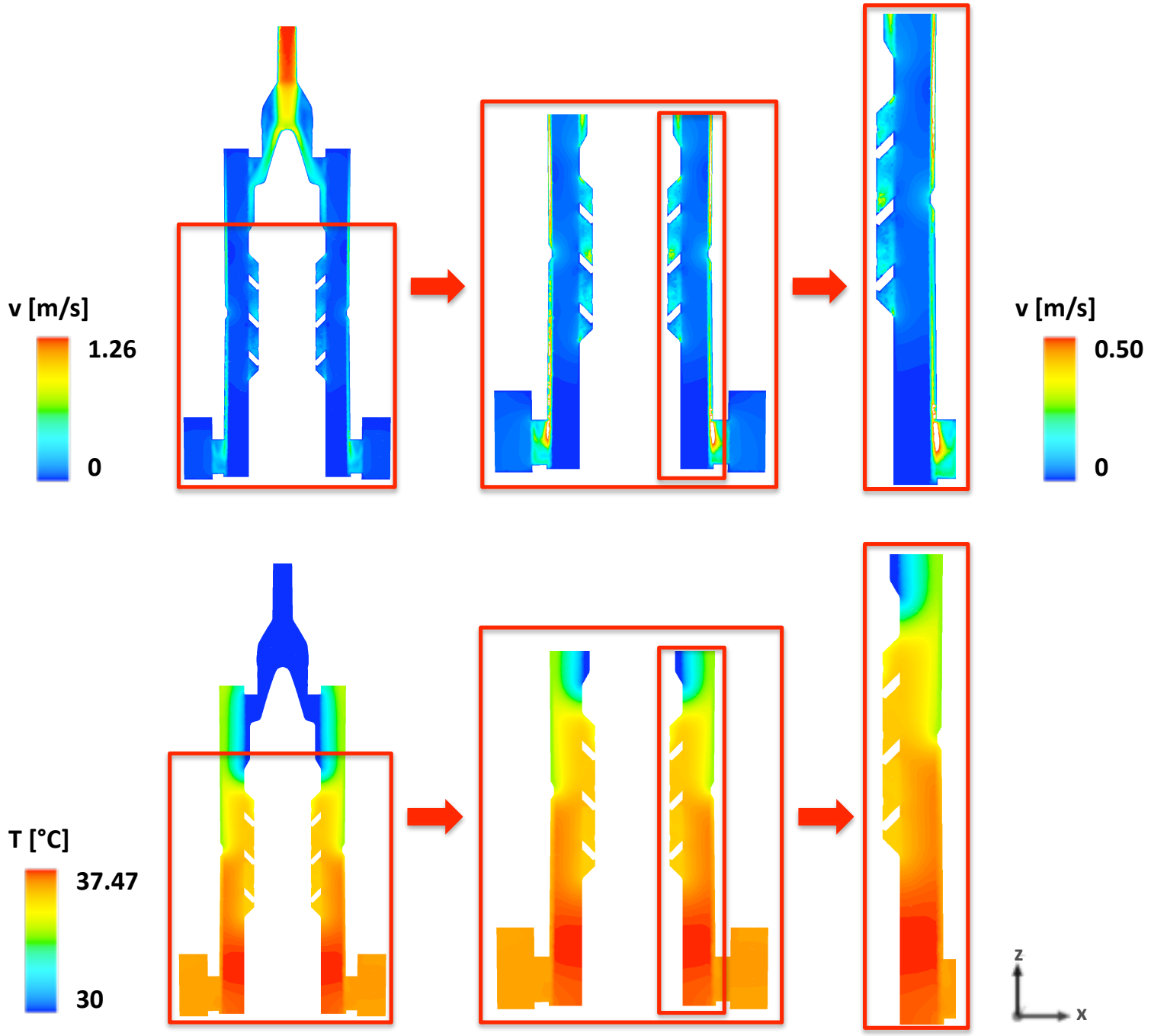
v [m/s]
1.26
0
v [m/s]
0.50
0
T [°C]
37.47
30
z
x
M4

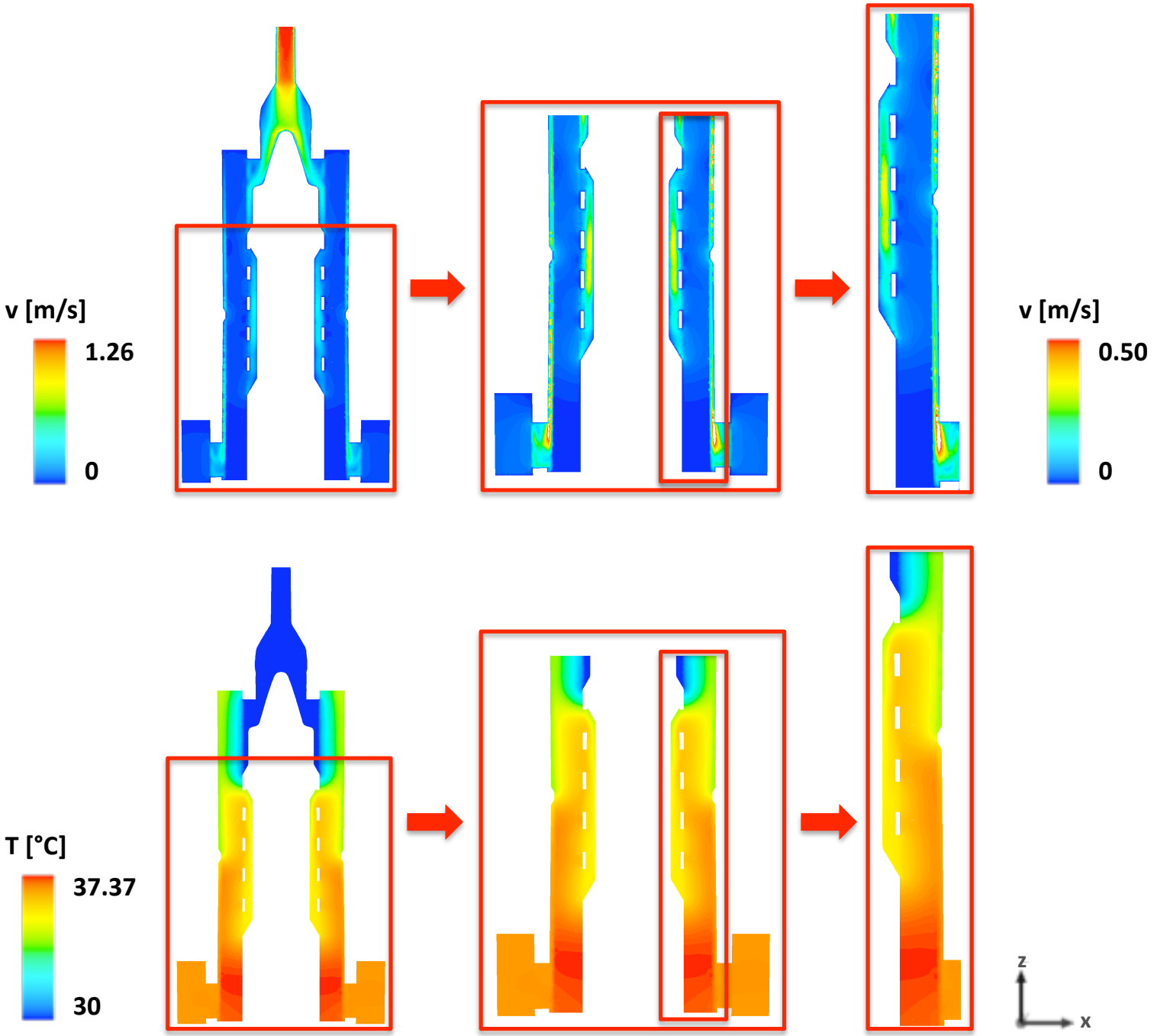
v [m/s]
1.26
0
v [m/s]
0.50
0
T [°C]
37.37
30
z
x
M5

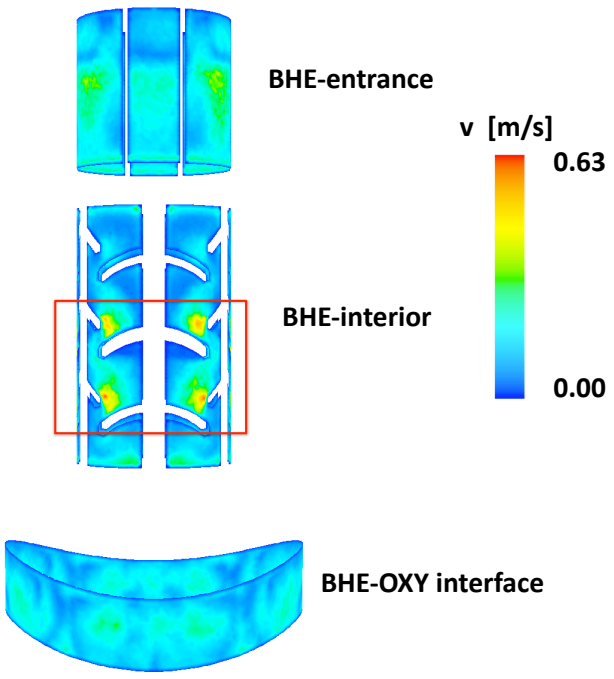
BHE-entrance
v [m/s]
0.63
BHE-interior
0.00
BHE-OXY interface

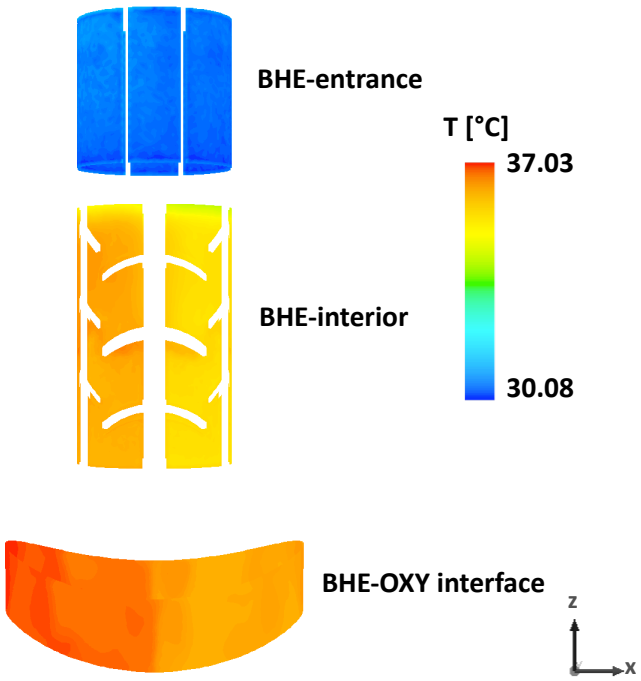
BHE-entrance
T [°C]
37.03
BHE-interior
30.08
BHE-OXY interface
z
x

A

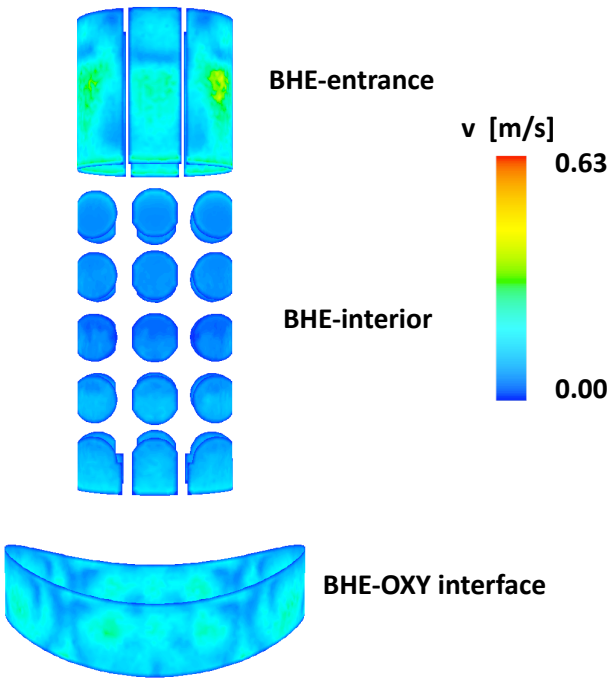
BHE-entrance
v [m/s]
0.63
BHE-interior
0.00
BHE-OXY interface

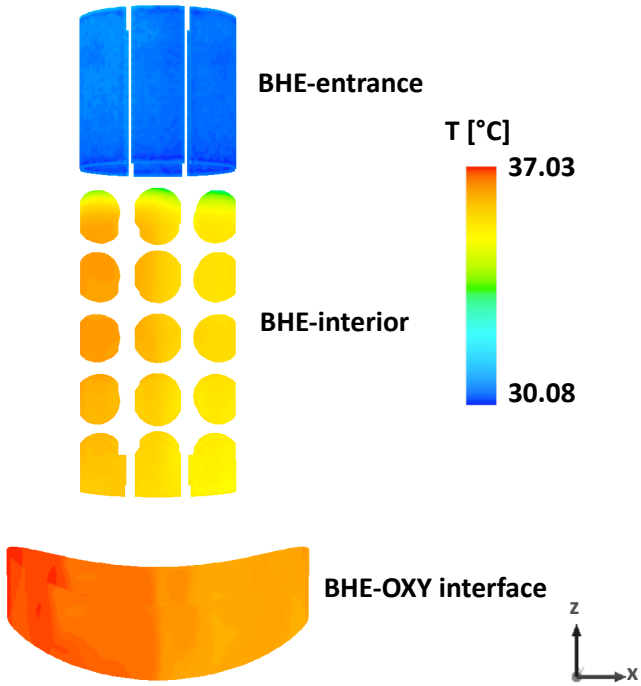
BHE-entrance
T [°C]
37.03
BHE-interior
30.08
BHE-OXY interface
z
x

B